Acta Mech 228, 617–630 (2017)
DOI 10.1007/s00707-016-1728-9

ORIGINAL PAPER

P. Intarit · T. Senjuntichai · J. Rungamornrat · R. K. N. D. Rajapakse

Penny-shaped crack in elastic medium with surface energy effects

Received: 6 May 2016 / Revised: 19 July 2016 / Published online: 7 October 2016

Abstract In this paper, a penny-shaped crack in an infinite elastic medium subjected to vertical pressure loading at the crack surface under the influence of surface stress is considered. The Gurtin–Murdoch continuum theory of elastic material surfaces is adopted, and the Hankel integral transform is employed to solve this axisymmetric boundary value problem. A set of simultaneous dual integral equations is solved by employing an appropriate numerical solution scheme. Selected numerical results are presented to portray the influence of the surface stress on the elastic field. Numerical results reveal that the surface stress has a significant influence on both stress and displacement fields. It is also found that the material becomes tougher with the presence of surface stress. In addition, the elastic field also shows size-dependent behavior deviating from the classical crack solution. The solutions presented in this study provide fundamental understanding of the influence of surface stress on fracture mechanics problems. It can also be used as a benchmark solution for the development of numerical techniques, such as FEM and BEM, for analysis of more complicated problems associated with cracks under the influence of surface stress.

1 Introduction

In recent years, studies on mechanics of nanomaterials and nanostructures have become increasingly important in various advanced engineering applications. In nanoscale structures, the influence of excess energy associated with the surface/interface atoms, called surface/interfacial free energy, is significant due to their high surface-to-volume ratio (e.g., see [1,2]). As a result, their mechanical behavior becomes size-dependent [3]. Atomistic simulations are powerful techniques to accurately analyze problems related to nanoscale systems; however, they require a very large computational effort. Thus, studying problems at the nanoscale based on the modified continuum mechanics concepts accounting for surface energy effects is an attractive option to obtain first approximations for this class of problems.

A rigorous theory based on the continuum mechanics concepts was developed to incorporate the surface and interfacial energy effects by Gurtin and Murdoch [4,5]. The surface is modeled as a zero thickness layer perfectly bonded to the underlying bulk material. Miller and Shenoy [6] examined the size effects of nanoscale plates and bars by employing the Gurtin–Murdoch continuum model and found that the results were in excellent agreement with those obtained from atomistic simulations. Several researchers analyzed nanoscale mechanics problems based on the Gurtin–Murdoch theory and neglected the out-of-plane components of surface stress (e.g., [7–12]). Later, Wang et al. [13] showed that the out-of-plane components of surface stress could be

P. Intarit · T. Senjuntichai (✉) · J. Rungamornrat
Department of Civil Engineering, Faculty of Engineering, Chulalongkorn University, Bangkok 10330, Thailand
E-mail: teerapong.s@chula.ac.th

R. K. N. D. Rajapakse
Department of Civil and Environmental Engineering, Carleton University, Ottawa K1S 5B6, Canada

significant even in the case of small deformations particularly for curved and rotated surfaces. Intarit et al. [14] considered the complete set of surface stresses in the analysis of a two-dimensional elastic layer under buried loading and found that the elastic field depends significantly on the surface elastic constants and residual surface stress. The complete version of the Gurtin–Murdoch model was also employed to study problems of an elastic layer under axisymmetric surface loading [15] and rigid frictionless indentation on an elastic half-space [16]. In addition, influence of surface stress is also important in problems involving soft elastic solids [17].

Fracture mechanics, which is concerned with the mechanical behavior of materials in the presence of cracks, has important practical applications. The study of cracks in devices and structures encountered in engineering applications is essential for both reliability and safety. Several crack problems were studied in the context of classical continuum theory in the presence of crack surface tension. Wu [18] and Wu and Wang ([19,20]) investigated the influence of surface tension on cracks and proposed that surface tension induced a pair of point loads at the crack tip. With the assumption of a blunt crack tip, Wang et al. [21] and Fu et al. [22] found that surface stress has a significant influence on stresses and displacements in the vicinity of crack tip, especially when the curvature of the crack tip is in the nanoscale. The solutions of Mode I, II and III cracks were derived with the consideration of surface stresses by assuming that the crack tip stresses are finite by Kim et al. [23,24]. The above studies dealt exclusively with plane crack (2-D) problems, whereas it is useful to examine more practical crack geometries such as penny-shaped cracks. The classical penny-shaped crack problem has been extensively studied (e.g., [25–28]), but studies related to its counterpart with surface elasticity based on the Gurtin–Murdoch theory are very limited. Recently, a numerical procedure based on the coupling of the standard finite element technique and the boundary integral equation method was proposed by Nguyen et al. [29] to investigate nanosized penny-shaped cracks in an infinite elastic medium under Mode I loading. However, their formulation accounts only for the residual surface tension and ignores the influence of the surface Lamé constants. A literature review indicates that an analytical solution for the penny-shaped crack problem with the complete version of the Gurtin–Murdoch theory has not yet been reported.

The influence of surface stresses on the elastic field of a penny-shaped crack in an infinite elastic medium is presented in this paper to provide a fundamental understanding of the behavior of nanoscale fracture. Axisymmetric vertical pressure loading is applied on the crack surface, and a perfectly sharp crack tip is assumed. The analysis is based on the complete version of the Gurtin–Murdoch theory of surface elasticity. The Hankel integral transform is used to reduce the problem to a set of dual integral equations together with an efficient numerical solution scheme for dual integral equations are employed to solve the boundary value problem involving non-classical boundary conditions associated with the surface stresses. Selected numerical results are presented to portray the influence of surface stresses on stress and displacement fields.

2 Governing equations and general solutions

Consider a penny-shaped crack with radius a in an infinite elastic medium and subjected to axisymmetric vertical loading $p(r)$ as shown in Fig. 1. In the present study, a sharp crack tip model is applied and, as a result, the crack geometry can be fully described by two geometrically identical, flat, circular surfaces on the plane $z = 0$. The elastic medium is governed by the Gurtin–Murdoch continuum theory [4,5]. In the absence of body forces, the equilibrium equations, constitutive laws and strain–displacement relations of an isotropic bulk material are given by

$$\sigma_{ij,j} = 0, \tag{1}$$

$$\sigma_{ij} = 2\mu\varepsilon_{ij} + \lambda\delta_{ij}\varepsilon_{kk}, \tag{2}$$

$$\varepsilon_{ij} = \frac{1}{2}\left(u_{i,j} + u_{j,i}\right), \tag{3}$$

where u_i, σ_{ij} and ε_{ij} denote, respectively, the components of displacement, stress and strain tensors; and μ and λ are Lamé constants of the bulk material.

On the crack surface, the equilibrium equation, constitutive laws and strain-displacement relations can be expressed as ([4,5]):

$$\sigma^s_{i\alpha,\alpha} + \sigma_{ij}n_j = 0, \tag{4}$$

$$\sigma^s_{\beta\alpha} = \tau^s\delta_{\beta\alpha} + 2\left(\mu^s - \tau^s\right)\varepsilon_{\beta\alpha} + \left(\lambda^s + \tau^s\right)\varepsilon_{\gamma\gamma}\delta_{\beta\alpha} + \tau^s u^s_{\beta,\alpha}; \quad \sigma^s_{3\alpha} = \tau^s u^s_{3,\alpha}, \tag{5}$$

$$\varepsilon^s_{\alpha\beta} = \frac{1}{2}\left(u^s_{\alpha,\beta} + u^s_{\beta,\alpha}\right), \tag{6}$$

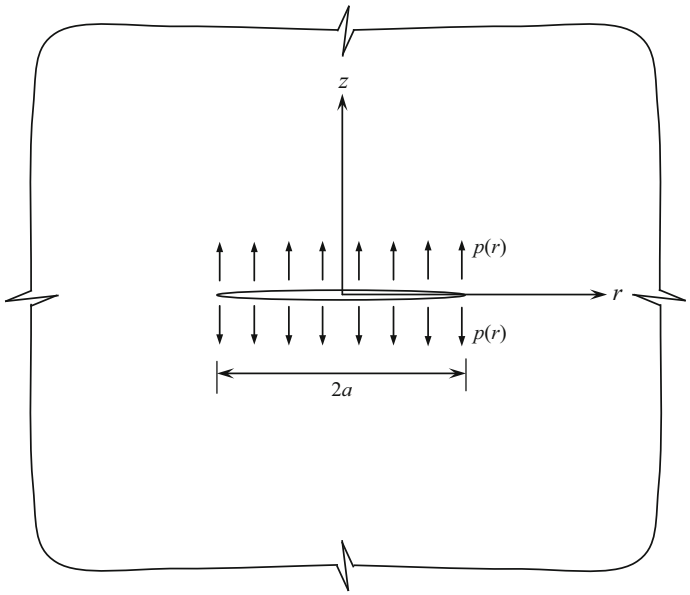

Fig. 1 Penny-shaped crack in infinite elastic medium under vertical loading

where the superscript 's' is used to denote the quantities corresponding to the surface; μ^s and λ^s are surface Lamé constants; τ^s is the residual surface stress (or surface tension) under unstrained conditions; n_i denotes the components of unit normal vector of the surface; and Greek subscripts take the value of 1 or 2, while the Latin subscripts vary from 1 to 3.

Due to the symmetry of the system shown in Fig. 1 about the z-axis, a cylindrical coordinate system (r, θ, z) is used in the formulation, and the elastic field is independent of θ, i.e., $u_\theta = 0$ and $\sigma_{r\theta} = \sigma_{z\theta} = 0$. The general solutions for the bulk stresses and displacements can be expressed by using Hankel integral transforms as [30]

$$\sigma_{rr} = \int_0^\infty \xi \left[\lambda \frac{\mathrm{d}^3\Phi}{\mathrm{d}z^3} + (\lambda + 2\mu)\,\xi^2 \frac{\mathrm{d}\Phi}{\mathrm{d}z}\right] J_0(\xi r)\,\mathrm{d}\xi - \frac{2(\lambda+\mu)}{r} \int_0^\infty \xi^2 \frac{\mathrm{d}\Phi}{\mathrm{d}z} J_1(\xi r)\,d\xi, \tag{7}$$

$$\sigma_{\theta\theta} = \lambda \int_0^\infty \xi \left[\frac{\mathrm{d}^3\Phi}{\mathrm{d}z^3} - \xi^2 \frac{\mathrm{d}\Phi}{\mathrm{d}z}\right] J_0(\xi r)\,\mathrm{d}\xi + \frac{2(\lambda+\mu)}{r} \int_0^\infty \xi^2 \frac{\mathrm{d}\Phi}{\mathrm{d}z} J_1(\xi r)\,\mathrm{d}\xi, \tag{8}$$

$$\sigma_{zz} = \int_0^\infty \xi \left[(\lambda + 2\mu) \frac{\mathrm{d}^3\Phi}{\mathrm{d}z^3} - (3\lambda + 4\mu)\,\xi^2 \frac{\mathrm{d}\Phi}{\mathrm{d}z}\right] J_0(\xi r)\,\mathrm{d}\xi, \tag{9}$$

$$\sigma_{rz} = \int_0^\infty \xi^2 \left[\lambda \frac{\mathrm{d}^2\Phi}{\mathrm{d}z^2} + (\lambda + 2\mu)\,\xi^2 \Phi\right] J_1(\xi r)\,\mathrm{d}\xi, \tag{10}$$

$$u_r = \frac{\lambda + \mu}{\mu} \int_0^\infty \xi^2 \frac{\mathrm{d}\Phi}{\mathrm{d}z} J_1(\xi r)\,\mathrm{d}\xi, \tag{11}$$

$$u_z = \int_0^\infty \xi \left[\frac{\mathrm{d}^2\Phi}{\mathrm{d}z^2} - \frac{\lambda + 2\mu}{\mu} \xi^2 \Phi\right] J_0(\xi r)\,\mathrm{d}\xi, \tag{12}$$

where

$$\Phi(\xi, z) = (A + Bz) e^{-|\xi| z}. \tag{13}$$

Note that $J_n(\xi)$ denotes the Bessel functions of the first kind of order n. In addition, A and B are arbitrary functions to be determined from the boundary conditions.

3 Solution of boundary value problem

Due to the symmetry about z-axis and the assumption that surface tension is constant, the boundary conditions on the crack surface ($z = 0$) can be expressed as

$$\sigma_{zz} + \tau^s \left(\frac{\mathrm{d}^2 u_z}{\mathrm{d}r^2} + \frac{1}{r}\frac{\mathrm{d}u_z}{\mathrm{d}r} \right) = -p\,(r) \quad \text{when } 0 < r < a, \tag{14}$$

$$u_z = 0 \quad \text{when } a < r < \infty, \tag{15}$$

$$\sigma_{rz} + \kappa^s \left(\frac{\mathrm{d}^2 u_r}{\mathrm{d}r^2} + \frac{1}{r}\frac{\mathrm{d}u_r}{\mathrm{d}r} - \frac{u_r}{r^2} \right) = 0 \quad \text{when } 0 < r < a, \tag{16}$$

$$\sigma_{rz} = 0 \quad \text{when } a < r < \infty, \tag{17}$$

where $\kappa^s = 2\mu^s + \lambda^s$ is a surface material constant.

It is worth noting that the boundary conditions (14) and (16) are only applicable to flat crack surfaces located on the plane $z = 0$ (resulting directly from the sharp crack tip assumption). The treatment of crack face conditions associated with non-flat crack surfaces resulting from other crack models (e.g., a blunt crack model) is not considered in the present study.

By substituting stresses and displacements from Eqs. (7)–(12) into Eqs. (14)–(17), the boundary conditions can be expressed as a set of simultaneous dual integral equations as

$$\int_0^\infty \sum_{j=1}^{2} c_{ij}\left(\overline{\xi}\right) f_j\left(\overline{\xi}\right) J_{\nu_i}\left(\overline{\xi}\overline{r}\right) \mathrm{d}\overline{\xi} = h_i\left(\overline{r}\right) \quad \text{when } 0 < \overline{r} < 1, \tag{18}$$

$$\int_0^\infty \sum_{j=1}^{2} \mathrm{d}_{ij}\left(\overline{\xi}\right) f_j\left(\overline{\xi}\right) J_{\nu_i}\left(\overline{\xi}\overline{r}\right) \mathrm{d}\overline{\xi} = g_i\left(\overline{r}\right) \quad \text{when } 1 < \overline{r} < \infty, \tag{19}$$

where $i = 1, 2$; $\overline{\xi} = \xi a$; $\overline{r} = r/a$, and

$$c = \begin{bmatrix} 2\left(\lambda+\mu\right)\frac{\overline{\xi}^4}{a^4} + \frac{\lambda+\mu}{\mu}\tau^s\frac{\overline{\xi}^5}{a^5} & 2\mu\frac{\overline{\xi}^3}{a^3} + 2\tau^s\frac{\overline{\xi}^4}{a^4} \\ 2\left(\lambda+\mu\right)\frac{\overline{\xi}^4}{a^4} + \frac{\lambda+\mu}{\mu}\frac{\overline{\xi}^5}{a^5}\kappa^s & -2\lambda\frac{\overline{\xi}^3}{a^3} + \frac{\lambda+\mu}{\mu}\kappa^s\frac{\overline{\xi}^4}{a^4} \end{bmatrix};$$

$$d = \begin{bmatrix} \frac{\lambda+\mu}{\mu}\frac{\overline{\xi}^3}{a^3} & 2\frac{\overline{\xi}^2}{a^2} \\ 2\left(\lambda+\mu\right)\frac{\overline{\xi}^4}{a^4} & -2\lambda\frac{\overline{\xi}^3}{a^3} \end{bmatrix};$$

$$f = \begin{bmatrix} A\left(\overline{\xi}\right) \\ B\left(\overline{\xi}\right) \end{bmatrix}; \quad v = \begin{bmatrix} 0 \\ 1 \end{bmatrix}; \quad h = \begin{bmatrix} -\overline{p}\left(\overline{r}\right) \\ 0 \end{bmatrix}; \quad g = \begin{bmatrix} 0 \\ 0 \end{bmatrix} \quad \text{and} \quad \overline{p}\left(\overline{r}\right) = ap\left(a\overline{r}\right).$$

Equations (18) and (19) can then be reduced to

$$\int_0^\infty \sum_{j=1}^{2} e_{ij}\left(\overline{\xi}\right) \psi_j\left(\overline{\xi}\right) J_{\nu_i}\left(\overline{\xi}\overline{r}\right) \mathrm{d}\overline{\xi} = h_i\left(\overline{r}\right) \quad \text{when } 0 < \overline{r} < 1, \tag{20}$$

$$\int_0^\infty \psi_i\left(\overline{\xi}\right) J_{\nu_i}\left(\overline{\xi}\overline{r}\right) \mathrm{d}\overline{\xi} = 0 \quad \text{when } 1 < \overline{r} < \infty, \tag{21}$$

where $\psi_i\left(\overline{\xi}\right) = \sum_{j=1}^{2} d_{ij}\left(\overline{\xi}\right) f_j\left(\overline{\xi}\right)$ and

$$e = cd^{-1} = \begin{bmatrix} \frac{2\mu(\lambda+\mu)}{\lambda+2\mu}\frac{\overline{\xi}}{a} + \tau^s\frac{\overline{\xi}^2}{a^2} & \frac{\mu}{\lambda+2\mu} \\ -\frac{\mu}{\lambda+2\mu}\kappa^s\frac{\overline{\xi}^2}{a^2} & 1 + \frac{\lambda+3\mu}{2\mu(\lambda+2\mu)}\kappa^s\frac{\overline{\xi}}{a} \end{bmatrix}.$$

To solve Eqs. (20) and (21), ψ_j is defined as [31]

$$\psi_j\left(\bar{\xi}\right) = \bar{\xi}^{1-\beta_j} \sum_{m=0}^{\infty} \varphi_{jm} J_{\nu_j+2m+\beta_j}\left(\bar{\xi}\right). \tag{22}$$

Equation (21) will be automatically satisfied due to the following properties of Sonine-Schafheitlin integrals [32]:

$$\int_0^{\infty} \bar{\xi}^{1-\beta_j} J_{\nu_j}\left(\bar{\xi}\bar{r}\right) J_{\nu_j+2m+\beta_j}\left(\bar{\xi}\right) \mathrm{d}\bar{\xi} = 0 \quad \text{when} \quad \bar{r} > 1, 2(\nu_j + m + 1) > 0 \text{ and } \beta_j \quad > 0. \tag{23}$$

Equation (20) can then be written as

$$\sum_{m=0}^{\infty} \sum_{j=1}^{2} \varphi_{jm} \int_0^{\infty} \bar{\xi}^{1-\beta_j} e_{ij}\left(\bar{\xi}\right) J_{\nu_i}\left(\bar{\xi}\bar{r}\right) J_{\nu_j+2m+\beta_j}\left(\bar{\xi}\right) \mathrm{d}\bar{\xi} = h_i\left(\bar{r}\right) \quad \text{when } 0 < \bar{r} < 1, \tag{24}$$

where φ_{jm} are the unknown coefficients to be determined.

Multiplying both sides of Eq. (24) by

$$\bar{r}^{1+\nu_i}\left(1-\bar{r}^2\right)^{\beta_i-1} \Im_k\left(\nu_i+\beta_i, 1+\nu_i, \bar{r}^2\right), \quad k = 0, 1, 2, \ldots, \mathrm{m},$$

and then integrating with respect to $\bar{r}$ from 0 to 1 yields [33]

$$\sum_{m=0}^{\infty} \sum_{j=1}^{2} \varphi_{jm} \int_0^{\infty} \bar{\xi}^{1-\beta_j-\beta_i} e_{ij}\left(\bar{\xi}\right) J_{\nu_i+2k+\beta_i}\left(\bar{\xi}\right) J_{\nu_j+2m+\beta_j}\left(\bar{\xi}\right) \mathrm{d}\bar{\xi} = Q_i\left(\nu_i, \beta_i, k\right), \tag{25}$$

where

$$Q_i\left(\nu_i, \beta_i, k\right) = \frac{\mathbf{\Gamma}(\nu_i + k + 1)}{2^{\beta_i-1}\mathbf{\Gamma}(\nu_i + 1)\mathbf{\Gamma}(k + \beta_i)} \int_0^1 h_i\left(\bar{r}\right)\bar{r}^{1+\nu_i}\left(1-\bar{r}^2\right)^{\beta_i-1} \Im_k\left(\nu_i+\beta_i, 1+\nu_i, \bar{r}^2\right) \mathrm{d}\bar{r}$$

and $\Im_n$ is the following Jacobi polynomial, which is defined in terms of hypergeometric series [32] as

$$\Im_n\left(\alpha, \gamma, x\right) = {}_2F_1\left(-n, \alpha + n; \gamma; x\right), \tag{26}$$

and ${}_2F_1(a, b; c; x)$ is the hypergeometric function.

The coefficients φ_{jm} can be obtained by solving Eq. (25). Note that the unspecified constant, β_j, in Eq. (25) must be positive to make the integral appearing in Eq. (25) to converge. Finally, the arbitrary functions A and B can be expressed as

$$A\left(\bar{\xi}\right) = \frac{\lambda\mu}{(\lambda+\mu)(\lambda+2\mu)} \frac{a^3}{\bar{\xi}^3}\left[\psi_1\left(\bar{\xi}\right) + \frac{a}{\lambda\bar{\xi}}\psi_2\left(\bar{\xi}\right)\right], \tag{27}$$

$$B\left(\bar{\xi}\right) = \frac{\mu}{(\lambda+2\mu)} \frac{a^2}{\bar{\xi}^2}\left[\psi_1\left(\bar{\xi}\right) - \frac{a}{2\mu\bar{\xi}}\psi_2\left(\bar{\xi}\right)\right]. \tag{28}$$

4 Numerical results and discussion

In this section, selected numerical results are presented to portray the influence of surface energy effects on the elastic field. The solutions for stresses and displacements can be obtained from Eqs. (7)–(12) with the arbitrary functions A and B given by Eqs. (27) and (28). In this study, the semi-infinite integrals in Eqs. (7)–(12) are evaluated by using a globally adaptive numerical quadrature scheme based on the 21-point Gauss-Kronrod rule [34]. The surface elastic constants can be obtained from atomistic simulations ([6,35,36]). In particular, Si [100] is chosen, in the numerical study, as a representative material with the bulk and surface properties $\lambda/\mu = 1.94$, $\mu = 40.2262$ GPa, $\lambda^s = 4.4939$ N/m, $\mu^S = 2.7779$ N/m and $\tau^s = 0.6506$ N/m [6]. In addition, following non-dimensional quantities, $r_0 = r/\Lambda_0$, $z_0 = z/\Lambda_0$ and $a_0 = a/\Lambda_0$ where $\Lambda_0 = \kappa^s/\mu$ is a reference length-scale parameter defined in terms of κ^s and μ of Si [100]. The numerical results in the present study

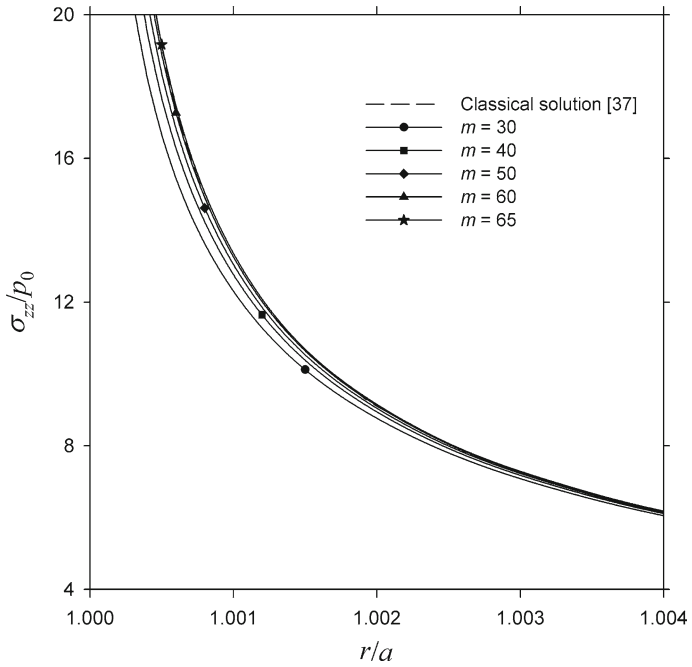

Fig. 2 Convergence of vertical stress solution in the vicinity of crack tip

correspond to the case of a penny-shaped crack in an infinite elastic medium subjected to a uniformly distributed vertical load, p_0, applied on the crack surface (i.e., $p(r) = p_0$ in Fig. 1).

The arbitrary functions A and B, given by Eqs. (27) and (28), are expressed as combinations of ψ_1 and ψ_2, which are given in terms of infinite series as shown in Eq. (22). The convergence and accuracy of the present solution are first verified by plotting the vertical stress in the vicinity of the crack tip to determine the appropriate number of terms, m, used in the series expansion defined in Eq. (22). Figure 2 shows a comparison of non-dimensional vertical stress in the vicinity of the crack obtained from the present scheme with no surface stress effects (i.e., $\kappa^s = \tau^s = 0$) for different m values with the classical solution given by Fabrikant [37]. It is seen that accurate results are obtained from the present solution scheme for $m \geq 60$. In Fig. 3, the present solutions for vertical stress and crack opening displacement are compared with the classical solutions provided by Fabrikant [37] and the numerical solutions given by Nguyen et al. [29], which ignore the surface Lamé constants (i.e., $\kappa^s = 0$), to confirm the high accuracy of the present solution scheme.

Figures 4 and 5 show the influence of surface energy effects on the elastic field in the vicinity of the crack. A non-dimensional crack radius of $a_0 = 1.0$ is considered in the numerical study. Variations of non-dimensional vertical stresses and non-dimensional crack opening displacement along the r-direction are shown in Figs. 4 and 5 for different values of surface residual stress (τ^s) and surface material constant (κ^s), respectively. Note that the broken lines in Fig. 4 denote the classical elasticity solution [37] and, during the variation of either τ^s or κ^s, all other material parameters associated with Si [100] remain unchanged.

The solutions for non-dimensional vertical stress close to the crack tip given in Figs. 4a and 5a show the effects of surface residual stress and surface elastic constants, respectively. Surface residual stress has a major influence on the crack tip vertical stress field, whereas the influence of surface elastic constants is negligible. Note that the difference observed in Fig. 5a between the classical elasticity solution and the present solution is primarily due to the effect of surface residual stress. It is observed that the presence of surface stress results in a substantial reduction in the crack tip vertical stress. Similar behavior was also observed in the 2-D crack solution by Kim et al. [24], in which the assumption of finite stress at the crack tip is considered. The present solutions in Figs. 4 and 5 also indicate that the order of singularity of stress is lower than the square root singularity corresponding to the classical solutions. This finding is consistent with that pointed out by several researchers (e.g., [38–42]); in particular, the stress singularity along the crack front reduces from the square root to logarithmic singularity when the surface stresses are accounted for in the mathematical model. The crack opening displacement solutions presented in Figs. 4b and 5b indicates that the magnitude of the crack opening displacement is substantially reduced due to the presence of surface stress. This is physically realistic

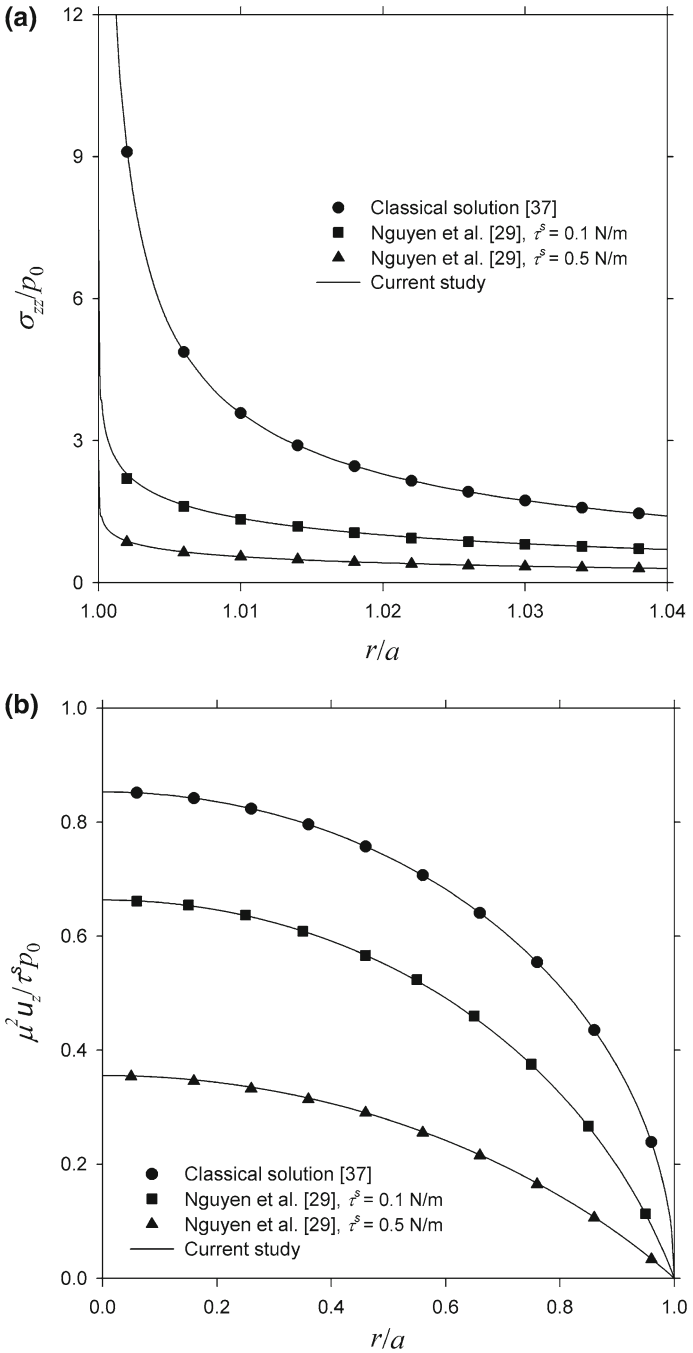

Fig. 3 Comparison with existing solutions: **a** vertical stress; **b** crack opening displacement

as a stretched (tensioned) crack face would be stiffer, similar to a cable under tension. Here again, the surface elastic constants show almost negligible influence on the crack opening displacement.

In Fig. 6, a set of numerical results is shown to demonstrate the size-dependent behavior of the present solution when the influence of surface energy effects (surface stress and surface elastic constants) is included. Solutions are presented for the radial variation of crack tip vertical stress and crack opening displacement across the crack surface for Si [100]. The corresponding non-dimensional solution for the classical elasticity case is also shown, and it is size-independent. It is found that as the crack size increases the current solution accounting for surface energy effects moves toward the classical solution. This is physically realistic as a

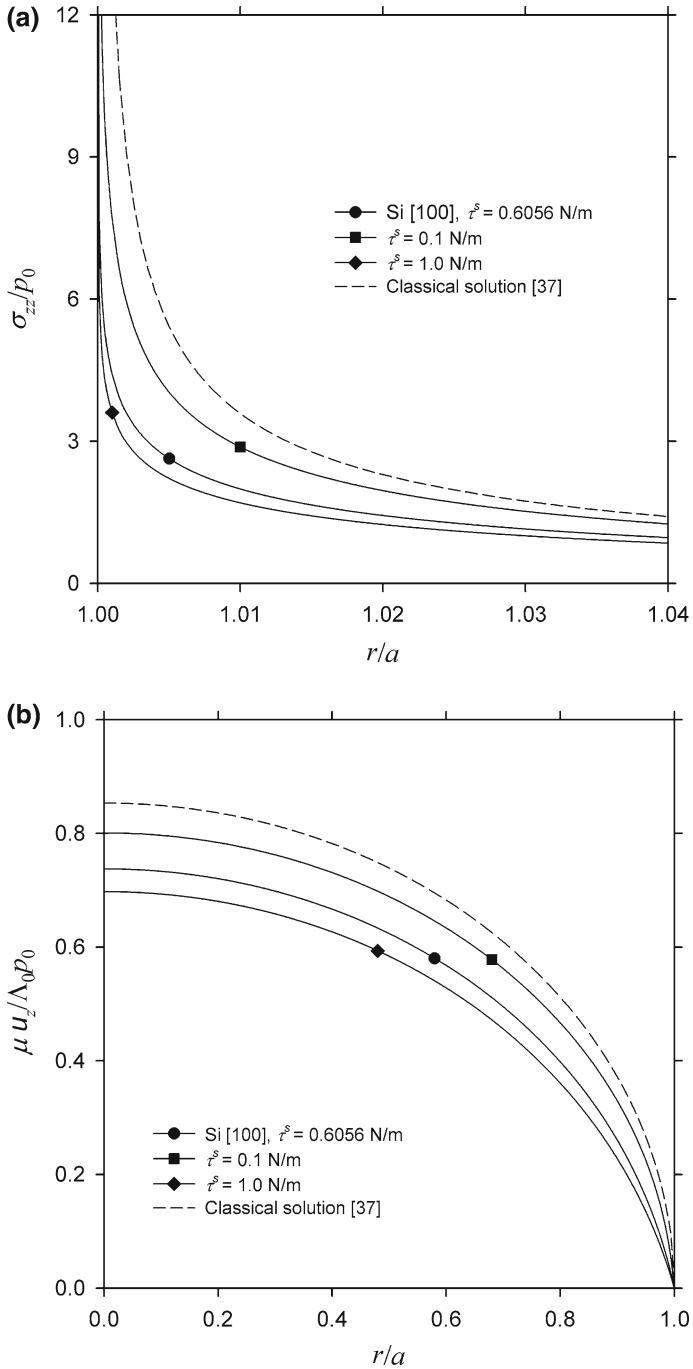

Fig. 4 Variation of elastic field for different magnitudes of surface residual stress (τ^s): **a** vertical stress; **b** crack opening displacement

stretched larger crack would show increasing crack opening displacements. The results show that a smaller crack has a lower crack tip stress and crack opening displacement.

The influence of surface residual stress and crack radius, respectively, on non-dimensional vertical stress at the vicinity of crack tip, i.e., at $r/a = 1.01$, and non-dimensional crack opening displacements at the center of the crack are presented in Figs. 7 and 8. The corresponding solutions for the classical elasticity case are also shown in both figures. It is evident from Fig. 7 that the residual surface stress (τ^s) displays strong influence on the crack tip stress and the central crack opening displacement. The stress and displacement both

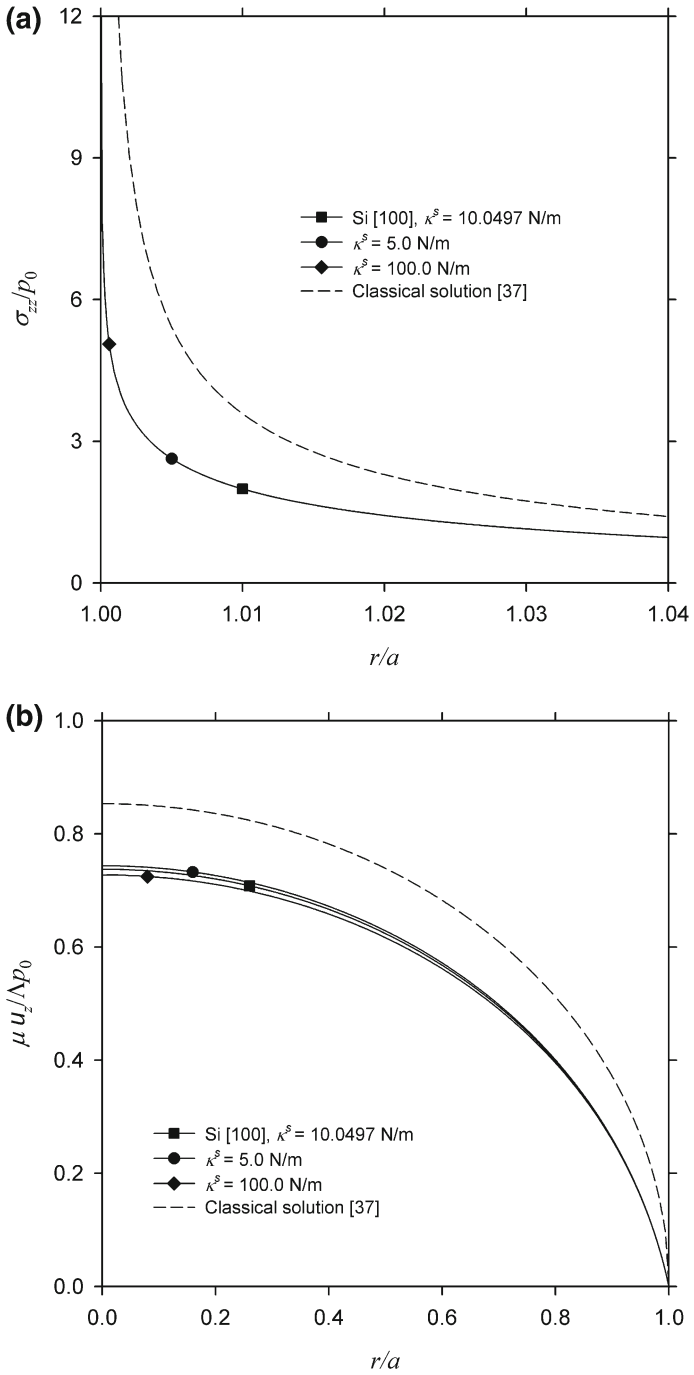

Fig. 5 Variation of elastic fields for different magnitudes of surface material constant (κ^s): **a** vertical stress; **b** crack opening displacement

decrease rapidly, from their classical elasticity counterparts, with an increase in the surface residual stress before approaching their limiting values. The size-dependent behavior due to the presence of surface stress effects can be clearly observed in Fig. 8. Both crack tip stress and central crack opening displacement obtained from the current model accounting for surface stress effects depend significantly on the crack size (a_0) for relatively small values of a_0. Such size dependency gradually vanishes as a_0 increases, and both stress and displacement converge to the corresponding classical solutions, which are shown as the broken lines in Fig. 8.

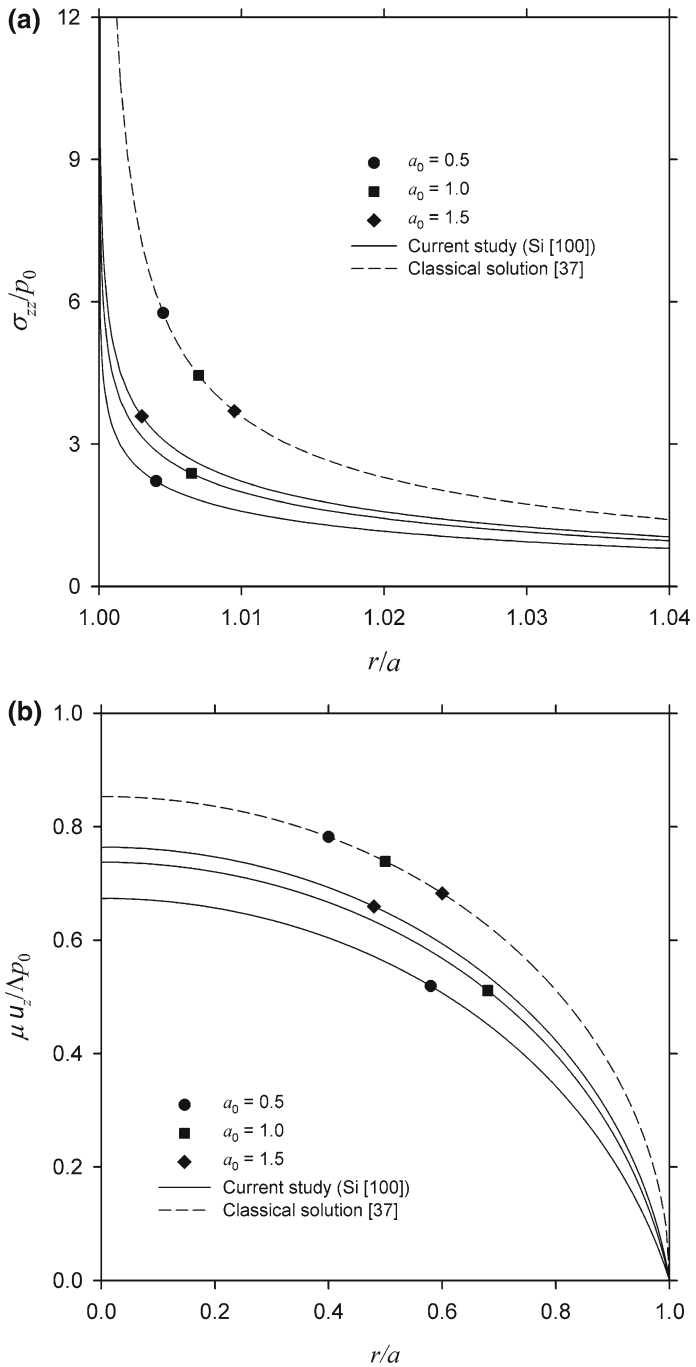

Fig. 6 Variation of elastic fields for different crack sizes (a_0): **a** vertical stress; **b** crack opening displacement

5 Conclusions

A theoretical model is presented for a penny-shaped crack in an infinite elastic medium in the presence of surface energy effects. The formulation is based on the Gurtin–Murdoch continuum theory and the application of Hankel integral transforms. It is shown that the solution to the crack problem can be reduced to a set of simultaneous dual integral equations similar to the classical elasticity case. The integral equation system is solved numerically and shows good convergence. The numerical results indicate that the surface energy effects have a significant influence on both stress and displacement fields of a medium with crack. The surface

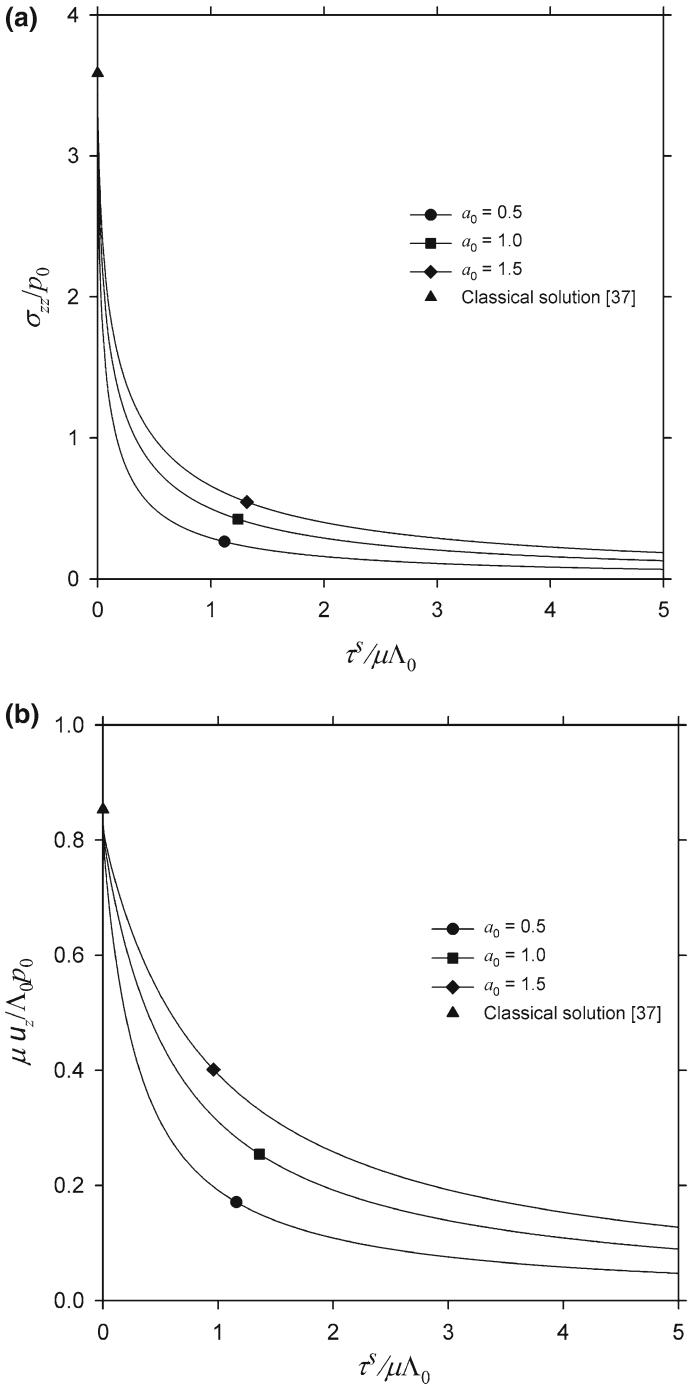

Fig. 7 Non-dimensional elastic fields under vertical loading against residual surface stresses (τ^s) for difference crack sizes (a_0): **a** vertical stresses in the vicinity of crack tip; **b** crack opening displacements at the center of the crack

residual stress has a far significant influence on the elastic field compared to the surface elastic constants. Surface residual stress reduces the crack opening displacement and the near-front vertical stress. As a result, the strength of the stress singularity along the crack front is clearly lowered when compared to the classical case. In contrast to the classical crack solution, the present study shows the substantial size dependency of a elastic field. Both crack tip stress field and crack opening displacement show a substantial dependency on the crack size and the magnitude of non-dimensional vertical stress, and crack opening displacement increase with increasing crack length. For larger cracks, the influence of surface energy is smaller. The present solution

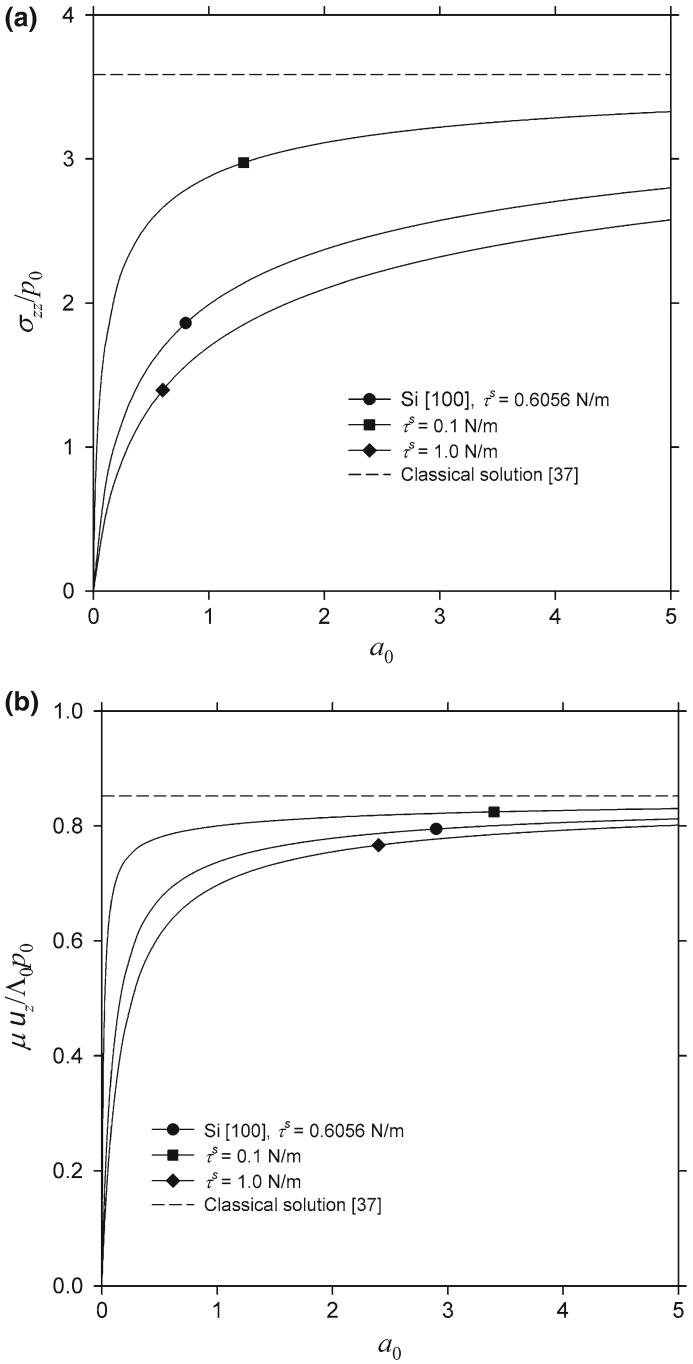

Fig. 8 Size dependency of non-dimensional **a** crack tip stress at $r/a = 1.01$; and **b** central crack opening displacement for different magnitudes of surface residual stress (τ^s)

can be used as a benchmark for assessing the accuracy of numerical models based on the finite element and boundary element methods that can be used to analyze more complicated crack problems in the presence of surface energy effects.

Acknowledgements The authors would like to acknowledge a research grant from the Thailand Research Fund (Grant No. BRG 5880017).

References

1. Yakobson, B.I.: Handbook of nanoscience, engineering and technology. In: Goddard, W.A., Brenner, D.W., Lyshevsk, S.E., Iafrate, G.J. (eds.) Nanomechanics. CRC Press, Boca Raton (2003)
2. Huang, Z.P., Wang, J.: A theory of hyperelasticity of multi-phase media with surface/interface energy effect. Acta Mech. **182**, 195–210 (2006)
3. Wong, E., Sheehan, P.E., Lieber, C.M.: Nanobeam mechanics: elasticity, strength and toughness of nanorods and nanotubes. Science **277**, 1971–1975 (1997)
4. Gurtin, M.E., Murdoch, A.I.: A continuum theory of elastic material surfaces. Arch. Rat. Mech. Anal. **57**, 291–323 (1975)
5. Gurtin, M.E., Murdoch, A.I.: Surface stress in solids. Int. J. Solids Struct. **14**, 431–440 (1978)
6. Miller, R.E., Shenoy, V.B.: Size-dependent elastic properties of nanosized structural elements. Nanotechnology **11**, 139–147 (2000)
7. Tian, L., Rajapakse, R.K.N.D.: Analytical solution for size-dependent elastic field of a nanoscale circular inhomogeneity. ASME J Appl. Mech. **74**, 568–574 (2007)
8. Zhao, X.J., Rajapakse, R.K.N.D.: Analytical solutions for a surface-loaded isotropic elastic layer with surface energy effects. Int. J. Eng. Sci. **47**, 1433–1444 (2009)
9. Intarit, P., Senjuntichai, T., Rajapakse, R.K.N.D.: Dislocations and internal loading in a semi-infinite elastic medium with surface stresses. Eng. Fract. Mech. **77**, 3592–3603 (2010)
10. Abdel Rahman, A.A., Mahmoud, F.F.: Analysis of nanocontact problems of layered viscoelastic solids with surface energy effects under different loading patterns. Acta Mech. **227**, 527–548 (2016)
11. Zhao, X.J., Rajapakse, R.: Elatic field of a nano-film subjected to tangential surface load: asymmetric problem. Eur. J. Mech.-A (Solids) **39**, 69–75 (2013)
12. Zhao, X.J.: Surface loading and rigid indentation of an elastic layer with surface energy effects. Master Thesis, University of British Columbia (2009)
13. Wang, Z.Q., Zhao, Y.P., Huang, Z.P.: The effects of surface tension on the elastic properties of nano structures. Int. J. Eng. Sci. **48**, 140–150 (2010)
14. Intarit, P., Senjuntichai, T., Rungamornrat, J., Rajapakse, R.K.N.D.: Surface elasticity and residual stress effect on the elastic field of a nanoscale elastic layer. Inter. Multi. Mech. **4**, 85–105 (2011)
15. Rungamornrat, J., Tuttipongsawat, P., Senjuntichai, T.: Elastic layer under axisymmetric surface loads and influence of surface stresses. Appl. Math. Model. **40**, 1532–1553 (2016)
16. Pinyochotiwong, Y., Rungamornrat, J., Senjuntichai, T.: Rigid frictionless indentation on elastic half space with influence of surface stresses. Int. J. Eng. Sci. **71**, 15–35 (2013)
17. He, L.H., Lim, C.W.: Surface Green functions for a soft elastic half-space: influence of surface stress. Int. J. Solids Struct. **43**, 132–143 (2006)
18. Wu, C.H.: The effect of surface stress on the configurational equilibrium of voids and cracks. J. Mech. Phys. Solids. **47**, 2469–2402 (1999)
19. Wu, C.H., Wang, M.L.: The effect of crack-tip point loads on fracture. J. Mech. Phys. Solids. **48**, 2283–2296 (2000)
20. Wu, C.H., Wang, M.L.: Configurational equilibrium of circular-arc cracks with surface stress. Int. J. Solids Struct. **38**, 4279–4292 (2001)
21. Wang, G.F., Feng, X.Q., Wang, T.J., Gao, W.: Surface effects on the near-tip stresses for Mode-I and Mode-III cracks. ASME J. Appl. Mech. **75**, 1–5 (2008)
22. Fu, X.L., Wang, G.F., Feng, X.Q.: Surface effects on the near-tip stress fields of a mode-II crack. Int. J. Fract. **151**, 95–106 (2008)
23. Kim, C.I., Schiavone, P., Ru, C.Q.: The effects of surface elasticity on an elastic solid with mode-III crack: complete solution. ASME J. Appl. Mech. **77**, 1–7 (2010)
24. Kim, C.I., Schiavone, P., Ru, C.Q.: Analysis of plane-strain crack problems (Mode-I & Mode-II) in the presence of surface elasticity. J. Elast. **104**, 397–420 (2011)
25. Sneddon, I.N.: The distribution of stress in the neighborhood of a crack in an elastic solid. Proc. R. Soc. (Lond.) **A187**, 226–260 (1946)
26. Florence, A.L., Goodier, J.N.: The liner thermoelastic problem of uniform heat flow distributed by a penny-shaped insulated crack. Int. J. Eng. Sci. **1**, 533–540 (1963)
27. He, M.Y., Hutchinson, J.W.: The penny-shaped crack and the plane strain crack in an infinite body of power-law material. ASME J. Appl. Mech. **48**, 830–840 (1981)
28. Fabrikant, V.I.: Inverse crack problem in elasticity. Acta Mech. **61**, 29–36 (1986)
29. Nguyen, T.B., Rungamornrat, J., Senjuntichai, T., Wijeyewickema, A.C.: FEM-SGBEM coupling for modeling of mode-I planar cracks in three-dimensional elastic media with residual surface tension effects. Eng. Anal. Bound. Elem. **55**, 40–51 (2015)
30. Sneddon, I.N.: Fourier Transforms. McGraw-Hill, New York (1956)
31. Erdogan, F., Bahar, L.Y.: On the solution of simultaneous dual integral equations. J. Soc. Ind. Appl. Math. **12**, 666–675 (1964)
32. Magnus, W., Oberhettinger, F.: Formulas and Theorems for the Functions of Mathematical Physics. Chelsea, New York (1954)
33. Tranter, C.J.: Integral Transforms in Mathematical Physics. Wiley, New York (1951)
34. Piessens, R., Doncker-Kapenga, E., Uberhuber, C.W., Kahaner, D.K.: QUADPACK: A Subroutine Package for Automatic Integration. Springer, Berlin (1983)
35. Shenoy, V.B.: Atomistic calculations of elastic properties of metallic fcc crystal surfaces. Phys. Rev. B. **71**, 094104 (2005)
36. Dingreville, R., Qu, J.: A semi-analytical method to compute surface elastic properties. Acta Mater. **55**, 141–147 (2007)
37. Fabrikant, V.I.: Applications of Potential Theory in Mechanics: A Selections of New Results. Kluwer Academic, Dordrecht (1989)

38. Sendova, T., Walton, J.R.: A new approach to the modeling and analysis of fracture through extension of continuum mechanics to the nanoscale. Math. Mech. Solids **15**(3), 368–413 (2010)
39. Walton, J.R.: A note on fracture models incorporating surface elasticity. J. Elast. **109**(1), 95–102 (2012)
40. Kim, C.I., Ru, C.Q., Schiavone, P.: A clarification of the role of crack-tip conditions in linear elasticity with surface effects. Math. Mech. Solids **18**(1), 59–66 (2013)
41. Walton, J.R.: Plane-strain fracture with curvature-dependent surface tension: Mixed-mode loading. J. Elast. **114**(1), 127–142 (2014)
42. Ferguson, L.A., Muddamallappa, M., Walton, J.R.: Numerical simulation of mode-III fracture incorporating interfacial mechanics. Int. J. Fract. **192**(1), 47–56 (2015)